The Astrophysical Journal, 671:1005–1012, 2007 December 10

THE NATURE OF RUNNING PENUMBRAL WAVES REVEALED

D. Shaun Bloomfield, Andreas Lagg, and Sami K. Solanki
Max-Planck-Institut für Sonnensystemforschung, Max-Planck-Strasse 2, 37191 Katlenburg-Lindau, Germany; bloomfield@mps.mpg.de
Received 2007 June 19; accepted 2007 September 5

ABSTRACT

We seek to clarify the nature of running penumbral (RP) waves: are they chromospheric trans-sunspot waves or a visual pattern of upward-propagating waves? Full Stokes spectropolarimetric time series of the photospheric Si I λ10827 line and the chromospheric He I λ10830 multiplet were inverted using a Milne-Eddington atmosphere. Spatial pixels were paired between the outer umbral/inner penumbral photosphere and the penumbral chromosphere using inclinations retrieved by the inversion and the dual-height pairings of line-of-sight velocity time series were studied for signatures of wave propagation using a Fourier phase difference analysis. The dispersion relation for radiatively cooling acoustic waves, modified to incorporate an inclined propagation direction, fits well the observed phase differences between the pairs of photospheric and chromospheric pixels. We have thus demonstrated that RP waves are in effect low-β slow-mode waves propagating along the magnetic field.

Subject headings: Sun: infrared — Sun: magnetic fields — sunspots — techniques: polarimetric — waves

Online material: color figures

1. INTRODUCTION

The term running penumbral (RP) wave was created by Zirin & Stein (1972) to describe chromospheric Hα velocity and intensity fronts that were observed moving out through sunspot penumbrae. Since then, a host of work has been carried out on reporting their properties (see, e.g., the series of papers by Christopoulou et al. 2000, 2001; Georgakilas et al. 2000), while their exact nature has remained unidentified. Currently, the two most likely possibilities for the form of these oscillatory disturbances are the following:

1. Trans-sunspot waves generated in the umbra (e.g., by umbral flashes) and limited to the chromospheric layer.
2. A "visual pattern" resulting from field-aligned waves propagating up from the photosphere.

To date, many findings point toward RP waves being due to the "visual pattern" scenario (for an extensive discussion of this topic see the recent review by Bogdan & Judge 2006). This seems especially likely now that Centeno et al. (2006) have successfully identified chromospheric 3 minute umbral oscillations as propagating, field-aligned, acoustic waves. However, recent work by Tziotziou et al. (2006, 2007) has not been able to decide between either of the two possible RP wave scenarios. Thus, the sum of the evidence is still not conclusive.

In this paper we use velocity time series observations that possess a twofold advantage over those of previous studies. The first is the simultaneous recording of photospheric and chromospheric lines, allowing the connection between velocities in the lower and upper atmosphere to be accurately investigated. The second is the retrieval of the magnetic vector at both heights in the atmosphere through the use of full Stokes spectropolarimetry, thus circumventing the need for any assumptions about the possible orientation of the magnetic field.

2. OBSERVATIONAL DATA

The data set used here was obtained from the main spot of active region NOAA 9451 on 2001 May 9 with the Tenerife Infrared Polarimeter (TIP; Martínez Pillet et al. 1999) attached to the German Vacuum Tower Telescope in Tenerife, Canary Islands. The $0.5'' \times 40''$ spectrograph slit was positioned across NOAA 9451 for approximately 70 minutes with no spatial scanning of the slit, while the solar image was kept stationary beneath the slit via a correlation tracking device (Ballesteros et al. 1996). The main umbra from this data set was previously analyzed and presented as data set 2 in the work of Centeno et al. (2006), so only a brief description of the observational setup and format of the data is supplied here. Note the correct heliographic coordinates of the observed sunspot are S22°, E20°.

The spectral region obtained in these observations was recorded with a wavelength sampling of 31 mÅ pixel^{-1} and includes the photospheric Si I λ10827.09 line, the upper chromospheric He I λ10830 multiplet (with triplet components at 10829.09, 10830.25, and 10830.34 Å), and the telluric H_2O line at 10832.11 Å. The TIP instrument was used to record simultaneous spectral images of the four Stokes parameters (I, Q, U, V) for each of the 0.4″ spatial pixels along the slit. Multiple images were co-added online to increase the signal-to-noise ratio, resulting in a final cadence of 2.1 s.

After dark current subtraction, flat-field correction, polarization calibration, and removal of polarization cross talk (Collados 2003), Stokes (I, Q, U, V) profiles were inverted separately for each line using the Milne-Eddington inversion code of Lagg et al. (2004). For the He I inversions an atmospheric model with one magnetic component was used, while a nonmagnetic component was included in the Si I inversions to account for stray light. A continuum intensity space-time plot of the time series is given in Figure 1, alongside absolute magnetic field strengths, line-of-sight (LOS) velocities, and magnetic field inclinations in solar coordinates (see § 3.2.1 for more details) retrieved by the Si I and He I inversions.

The Si I and He I LOS velocities retrieved from the inversions both show systematically decreasing velocity (i.e., blueshift) with time. This trend arises from the relative motion along the observer's LOS caused by the Earth's rotation, as these observations were obtained during local morning. Simple linear fits proved a suitable approximation to the trends and LOS velocity

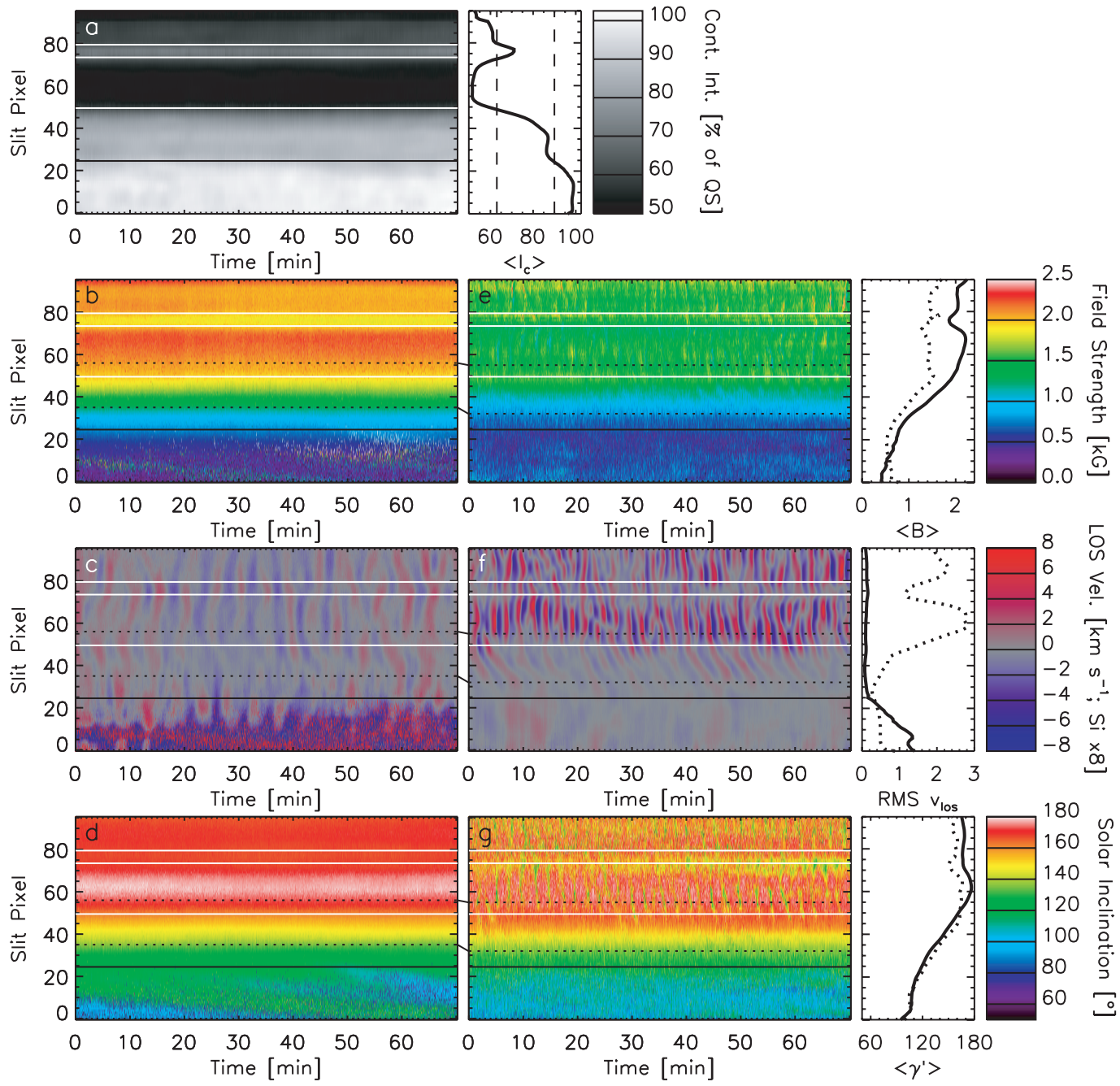

FIG. 1.—Space-time plots of (*a*) continuum intensity at 10825.7 ± 0.3 Å, absolute magnetic field strengths in (*b*) Si I and (*e*) He I, LOS velocities in (*c*) Si I and (*f*) He I (*f*), and magnetic inclinations in solar coordinates from (*d*) Si I and (*g*) He I (*g*). Si I and He I velocities both have linear background trends removed; Si I velocities are scaled up by a factor of 8 to the dynamic range of the He I velocities. Upper solid white lines enclose a light bridge in the umbra, while the lower white (black) line marks the umbral/penumbral (penumbral/quiet Sun) boundary. Temporal averages of the parameters (rms values for LOS velocities) are shown in the rightmost panels for both Si I and He I (*solid and dotted curves, respectively*). Regions of spatial pixels paired between Si I and He I (see § 3.2.1) are marked by horizontal dotted lines in panels *b*–*g*. Note oscillations in He I field strength and inclination are not real, but result from misfitting of the Stokes profiles associated with wave shocking. Observed shock profiles require two components; the single component inversion used here retrieves weakened, more inclined fields. However, the He I velocities retrieved still represent the general plasma motion.

time series from each spatial pixel had these linear background trends removed prior to any form of temporal analysis.

3. ANALYSIS METHOD

Fourier phase difference analysis is a useful tool through which the propagation characteristics of waves may be determined. The form of analysis used here is based on the standard Fourier equations that are discussed in depth by Krijger et al. (2001). This technique has been used extensively in the past for various solar studies (e.g., Jensen & Orrall 1963; Sivaraman 1973; Lites 1984; Wikstøl et al. 2000), and it remains one of the most robust methodologies in use.

The phase difference spectrum, $\Delta\phi(\nu)$, between two temporal signals measures the phase lag at discrete frequencies. For signals separated by some spatial distance, this lag is the cycle time that it takes different frequency components to travel from the first location to that of the second. When waves propagate between two locations in a normally dispersive medium,

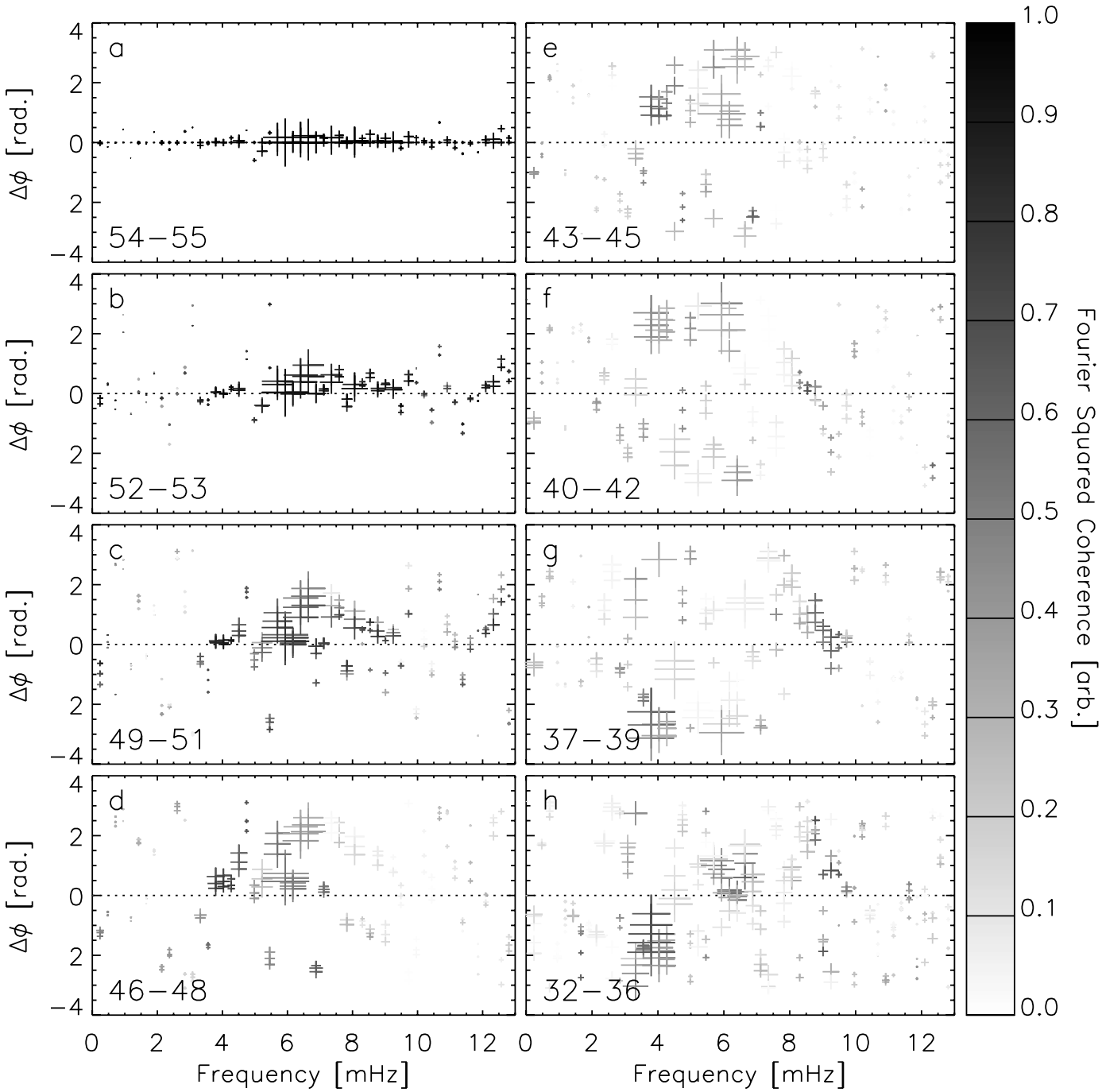

FIG. 2.—Phase-difference spectra between He I LOS velocity in the umbra and those at increasing distance into the penumbra. Symbol size and shading denote cross-spectral power and squared coherence, respectively. Panels show groups of phase difference spectra calculated between umbral pixel 55 and the pixel numbers listed in the lower left corners, moving from cases concerning pixels closest to (*a*) the umbra/penumbra boundary toward (*h*) those in the middle penumbra. The Fourier squared coherence "noise" level has a value of 0.2 for randomly distributed phase differences in these data. [*See the electronic edition of the Journal for a color version of this figure*.]

phase-difference spectra will show zero phase difference at low frequencies (where waves are evanescent and not propagating) followed by phase differences which increase in magnitude at higher frequencies (as high-frequency components travel more slowly than low-frequency components).

The Fourier phase coherence spectrum, $C^2(\nu)$, between two signals is a measure of the quality of phase difference variation. However, unless averaging in frequency is performed, the coherence between two Fourier components will be unity irrespective of the phase differences. The Fourier squared coherence of randomly distributed phase differences then approaches $1/n$ for averaging over n points in frequency. In this work coherence values are calculated using an average over five frequency intervals, providing a "noise" level of 0.2 for randomly distributed (i.e., uncorrelated) phase differences. In the following phase difference diagrams, Fourier squared coherence is represented by the degree of symbol shading (white for 0; black for 1), while the symbol size represents the cross-spectral power—a measure of the covariance between the Si I and He I LOS velocity signals.

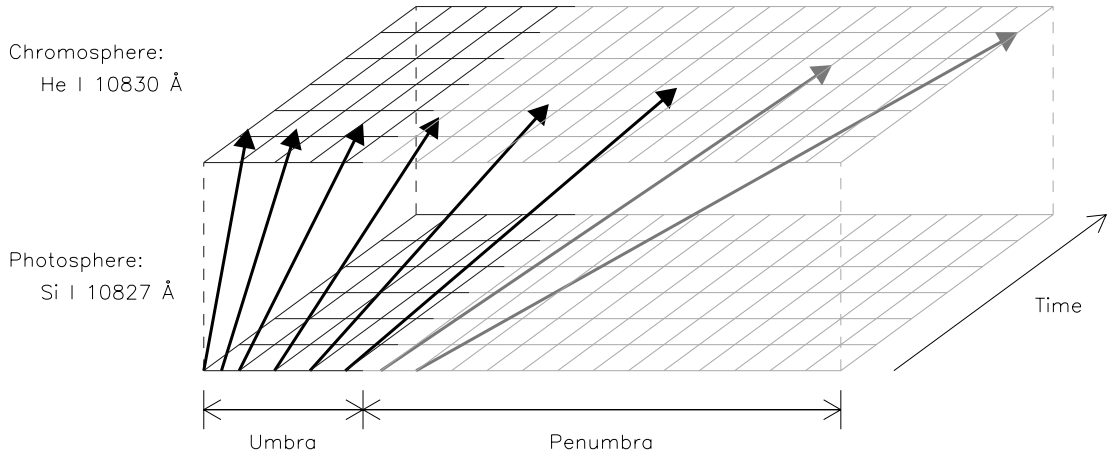

FIG. 3.—Cartoon schematic space-time diagram illustrating the form of pixel coupling between the photosphere and chromosphere for the case of field-aligned, upward-propagating waves presented in § 3.2. Dark (light) grids denote umbral (penumbral) pixels, while dark (light) arrows indicate magnetic lines of force (i.e., wave paths) linking back to the photospheric umbra (penumbra). Note increasing delays in wave front arrival time at the chromospheric sampling height because of increased propagation lengths along more inclined field lines. The horizontal and vertical axes are not to scale, resulting in magnetic field inclinations that appear different to the values actually retrieved from the Stokes inversions.

3.1. *Trans-Sunspot Wave*

If RP waves are due to waves propagating across the sunspot chromosphere, spectra calculated between the chromospheric LOS velocities from the umbra and those from pixels at sequentially greater distances into the penumbra should show phase difference values increasing linearly with frequency, becoming steeper with greater spatial separation of the signals. In this analysis, Fourier phase differences and coherences were calculated between the He I LOS velocity from pixel 55 (located in the umbra) and the He I LOS velocities from pixels at increasing distances into the penumbra.

Figure 2 shows the output from such an analysis, where phase difference spectra between the He I LOS velocity from pixel 55 and those pixel numbers listed in each panel are overplotted. For example, panel *a* contains $\Delta\phi_{\mathrm{He}(t,55)\rightarrow\mathrm{He}(t,55)}$ and $\Delta\phi_{\mathrm{He}(t,55)\rightarrow\mathrm{He}(t,54)}$, while panel *b* contains $\Delta\phi_{\mathrm{He}(t,55)\rightarrow\mathrm{He}(t,53)}$ and $\Delta\phi_{\mathrm{He}(t,55)\rightarrow\mathrm{He}(t,52)}$, where $\mathrm{He}(t, Y)$ denotes the temporal He I LOS velocity signal from spatial pixel *Y*. Although groups of phase difference spectra are overplotted to increase the clarity of any relations, no clear form of propagating wave behavior is seen. Note that around 4 mHz (i.e., 4 minute period) values of increasing phase difference are observed when moving into the penumbra. However, the finding is marginal since the values of Fourier squared coherence in the spectra rapidly approach the "noise" level of 0.2 for randomized phase differences.

3.2. *Upward-Propagating Waves*

Although a number of differing forms of propagating wave can exist in the outer atmosphere of a sunspot (e.g., fast/slow magnetoacoustic and Alfvén waves), we restrict our analysis of upward-propagating waves to that of field-aligned acoustic waves, as these were shown by Centeno et al. (2006) to describe the phase behavior of 3 minute waves in sunspot umbrae. The extension of these waves from traveling along near-vertical field lines in the umbra to traveling along inclined field lines which expand out over the penumbra is not unexpected since

1. the magnetic field inclination increases smoothly from the umbral center out through the penumbra (Figs. 1*d* and 1*g*); and
2. the photospheric LOS velocity signals are fairly coherent across the umbra/penumbra boundary (Fig. 1 *c*).

To study the possible propagation of field-aligned waves between two atmospheric heights we must first accurately determine the photospheric pixels that provide the lower atmospheric signal for the chromospheric pixels which lie above the penumbra. This is necessary because the field is significantly inclined here (Figs. 1*d* and 1*g*) and velocity signals in the upper atmosphere will be spatially removed from their originating photospheric pixels. The expected picture for field-aligned, upward-propagating waves is indicated in the schematic diagram of Figure 3, where increasingly inclined field lines at the photosphere reach further into the chromospheric penumbra.

3.2.1. *Atmospheric Height Coupling*

In order to correctly pair spatial pixels between the photosphere and the chromosphere we require reliable determination of the magnetic field vector in solar coordinates. This is complicated by the 180° azimuthal ambiguity, whereby two equally valid but opposite azimuth orientations exist in the observer's coordinate frame. This uncertainty in the field azimuth impacts on the whole magnetic vector; the two differing azimuthal solutions yield different solar inclinations, γ'.

To overcome this ambiguity we have implemented a "smoothest magnetic vector" form of ambiguity solution. Namely, a pixel region with the most realistic solution is selected as a trusted starting point (e.g., in the umbra where the true solution should be closest to vertical). Moving away from this seed region, either the 0° or 180° azimuth solution is chosen on a pixel-by-pixel basis to minimize the spatial variation in the three orthogonal components of the solar magnetic vector (B_x, B_y, B_z), where the *z*-direction is normal to the solar surface. The field inclinations achieved in solar coordinates are shown in Figures 1*d* and 1*g* for the inversion results from Si I and He I, respectively.

Spatial pixels were then paired between the photosphere and chromosphere using the temporal averages of Si I inclinations in the solar coordinate frame[1], $\langle\gamma'_{\mathrm{Si}}\rangle$. Coupled with an expected height separation, ΔH, these inclinations provide pixel offsets between photospheric and chromospheric pixel pairs in the direction

[1] Inclinations determined by the Si I inversion were chosen for this task because the greater signal-to-noise ratio achieved in this line means that its magnetic vector, and hence solar inclination, is more reliably determined in comparison to that from the He I inversion.

TABLE 1
SPATIAL PAIRINGS BETWEEN Si I AND He I PIXELS AND THEIR CORRESPONDING MAGNETIC FIELD INCLINATIONS IN SOLAR COORDINATES

	Si I		He I		
PAIR	Spatial Pixel	Inclination (deg)	Spatial Pixel	Inclination (deg)	NOTES[a]
1	56	172	55	165	*a*
2	55	170	54	165	*a*
3	54	169	53	164	*b*
4	53	167	52	164	*b*
5	52	165	51	163	*c*
6	51	163	50	163	*c*
7	50	161	49	163	*c*
8	49	160	48	163	*d*
9	48	158	47	163	*d*
10	47	157	46	162	*d*
11	47	157	45	161	*e*
12	46	155	44	160	*e*
13	45	153	43	158	*e*
14	44	151	42	156	*f*
15	43	150	41	153	*f*
16	42	148	40	150	*f*
17	41	146	39	147	*g*
18	40	145	38	145	*g*
19	39	143	37	143	*g*
20	39	143	36	142	*h*
21	38	141	35	139	*h*
22	37	139	34	138	*h*
23	36	136	33	136	*h*
24	35	134	32	135	*h*

[a] Panel of Fig. 4 in which the resulting Fourier phase difference spectra are overplotted.

along the slit by $\Delta S = |\tan \langle \gamma'_{\rm Si} \rangle| \cos \alpha \, \Delta H / s_{\rm pix}$, where ΔH was taken as 1000 km (following the findings of Centeno et al. 2006 for this sunspot umbra), $s_{\rm pix}$ is the spatial sampling of the slit ($\approx$300 km pixel^{-1}), and α is the angle between the field azimuth and the slit direction. Regions of pixels paired together in this work are outlined in panels *b–g* of Figure 1 by dotted lines, while details of the pixel pairs are provided in Table 1 with their corresponding field inclinations. Although this approach uses the simplifying assumption that the magnetic field remains essentially linear between the two formation heights (i.e., there is no field curvature), it is somewhat justified by the resulting pixel pairs in Table 1 having inclinations that differ by $\leq 7^\circ$, i.e., $\langle \gamma'_{\rm Si} \rangle \approx \langle \gamma'_{\rm He} \rangle$.

The Fourier phase difference spectra resulting from these dual-height pixel pairs are presented in Figure 4, where spectra from groups of adjacent pixel pairs are again overplotted to enhance any relations. In contrast to the trans-sunspot case depicted in Figure 2, the expected form of phase difference variation due to propagation (i.e., increasing values of phase difference with frequency) is clearly apparent in most of the panels. In addition, throughout panels *a–g* Fourier squared coherence values remain reasonably high.

3.2.2. *Dispersion Relation Comparison*

We make use of the equations provided in Centeno et al. (2006) that describe the dispersion relation for vertical acoustic waves propagating in the presence of a vertical magnetic field within a stratified isothermal atmosphere with radiative cooling. The equations were modified for this work to simplistically mimic the first-order effects that acoustic-like (low-β slow-mode) waves would experience when propagating along inclined field lines instead of purely vertically in a vertical magnetic field—i.e., $\cos \gamma'$ reduced gravity and $1/\cos \gamma'$ increased path length.

The solid curves in Figure 4 were calculated using the measured values of field inclination in solar coordinates along with the temperature (4000 K), radiative cooling time (55 s), and vertical height separation (1000 km) given by Centeno et al. (2006) for this sunspot umbra. Although only a simple approximation to the expected dispersion relation for such waves, these curves show an encouraging association with the measured data points.

4. DISCUSSION

In this section we present our findings in the context of results from previous studies in an attempt to provide answers to a few of the outstanding issues surrounding the relationship that RP waves share with other forms of sunspot waves.

It has been long known that sunspot chromospheres oscillate at differing periods in different spatial regions (Giovanelli 1972). Figure 5 displays the variation of Fourier power from the Si I and He I LOS velocities in the form of space-frequency diagrams. Individual power spectra from each spatial pixel have been normalized to the variance of the respective time series, resulting in white noise having power of 1 and 18.4 being the 99.99% significance level of Poisson noise. Normalization was performed to aid in the comparison of spectral profiles between spatial regions that exhibit vastly different LOS velocity amplitudes. Rather than indicating some form of physical discontinuity (cf. Tziotziou et al. 2006, 2007), the change from dominant chromospheric 3 minute power to longer periods near the umbra/penumbra boundary in Figure 5*b* may just result from the magnetic field inclination becoming large enough to allow photospheric low-frequency (i.e., 5 minute *p*-mode) power to tunnel through the higher frequency acoustic cutoff (5.2 mHz) at the temperature minimum (De Pontieu et al. 2004). We note that the classical interpretation of an acoustic cutoff is effectively negated by the

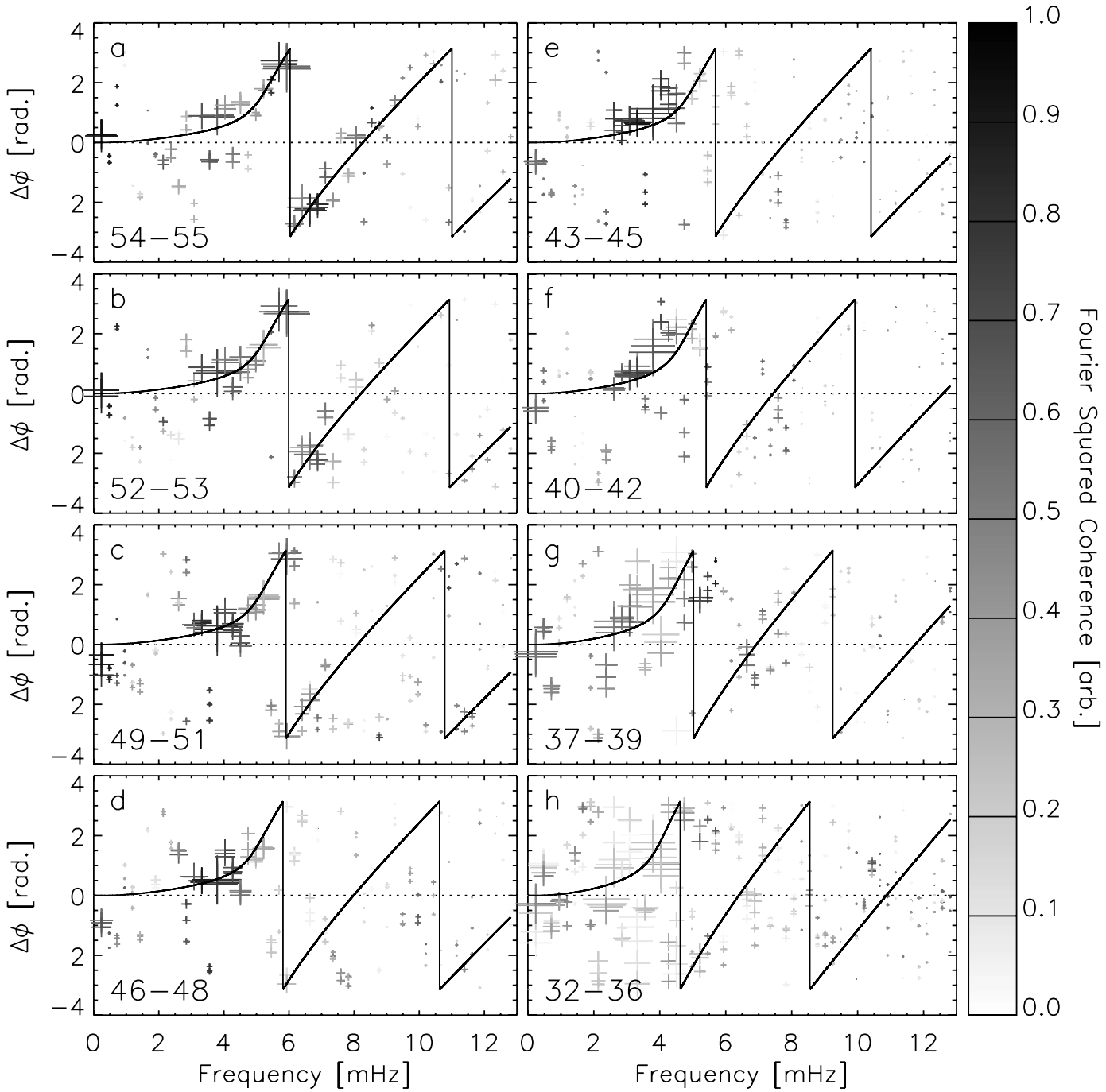

FIG. 4.—Same as Fig. 2, but for spatially offset dual-height pairs of photospheric and chromospheric pixels. Curves show modified acoustic dispersion curves using the measured Si I field inclinations. [*See the electronic edition of the Journal for a color version of this figure.*]

inclusion of radiative cooling in the modeled dispersion relation of § 3.2.2, which allows wave reflection and transmission at all frequencies. However, the dominant chromospheric frequency in Figure 5*b* is modified by the magnetic field inclination, closely following the strong-field limit $\cos\gamma'$ relation of Bel & Leroy (1977). Power existing below the cutoff may be explained by the gradual transition from mainly reflected to transmitted waves around the cutoff (i.e., the slow turn-up in the curves of Fig. 4). Another possibility is the presence of unresolved structure in the chromospheric penumbra (Rüedi et al. 1995), consisting of either two spatially separated distributions of field inclination along the LOS or an uncombed magnetic field configuration (Lagg et al. 2007). If the more vertical distribution has the measured field inclinations and the other has values $\sim 20^\circ$ larger, the acoustic cutoff curve in Figure 5*b* could be pulled to even lower frequencies. At larger field inclinations (i.e., further into the penumbra) little evidence is found of 3 minute waves because power at the 5 minute period vastly exceeds that at 3 minutes in the underlying photosphere (Fig. 5*a*).

The termination of 3 minute wave patterns at the umbra/penumbra boundary noted by Kobanov & Makarchik (2004) and Kobanov et al. (2006) and the fact that not all 3 minute wave fronts can be traced out from the umbra into the penumbra has been used to suggest that RP waves are not associated with similar waves in the umbra. A simple check for the linkage of either 3 or 5 minute waves between the chromospheric umbra

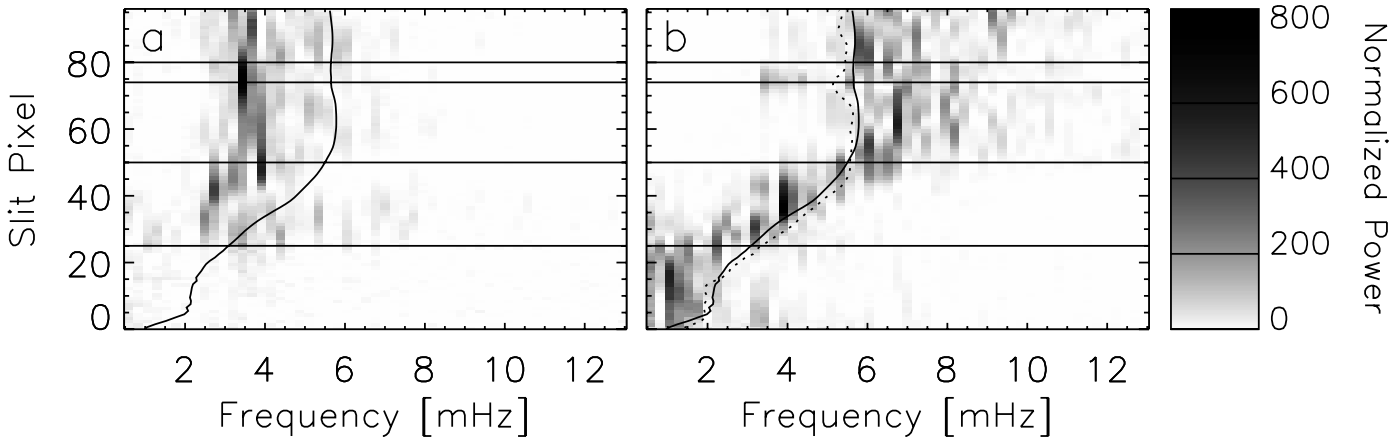

FIG. 5.—Space-frequency plots of (*a*) Si I and (*b*) He I velocity power. Spectra from each spatial pixel have been normalized to the variance of the corresponding time series; white noise has power of unity and 18.4 is the 99.99% significance level. Overlaid solid (dotted) curves are the acoustic cutoff modified by the Si I (He I) inclinations, while horizontal lines mark the same boundaries as in Fig. 1. [*See the electronic edition of the Journal for a color version of this figure*.]

and penumbra can be made by bandpass filtering the He I velocity time series. The spatial variation of He I LOS velocities through the umbra and penumbra is presented in Figure 6 before and after filtering in the period ranges 2.5–3.5 and 4.5–5.5 minutes. It is clear that each of the 3 minute umbral wave fronts has a rapidly diminishing counterpart in the penumbra (Fig. 6*b*), while each of the 5 minute (i.e., RP) wave fronts has an only somewhat weaker counterpart within the umbra (Fig. 6*c*). These findings once again support the picture of a continuous variation of RP wave behavior through the entirety of the sunspot atmosphere.

If RP waves are indeed the "visual pattern" of upward-propagating waves we expect that the wave velocity amplitude along the field would be essentially constant through the penumbra, because each wave front will have experienced the same degree of wave growth caused by the decrease of density with altitude. Examination of the unfiltered He I LOS velocity signal

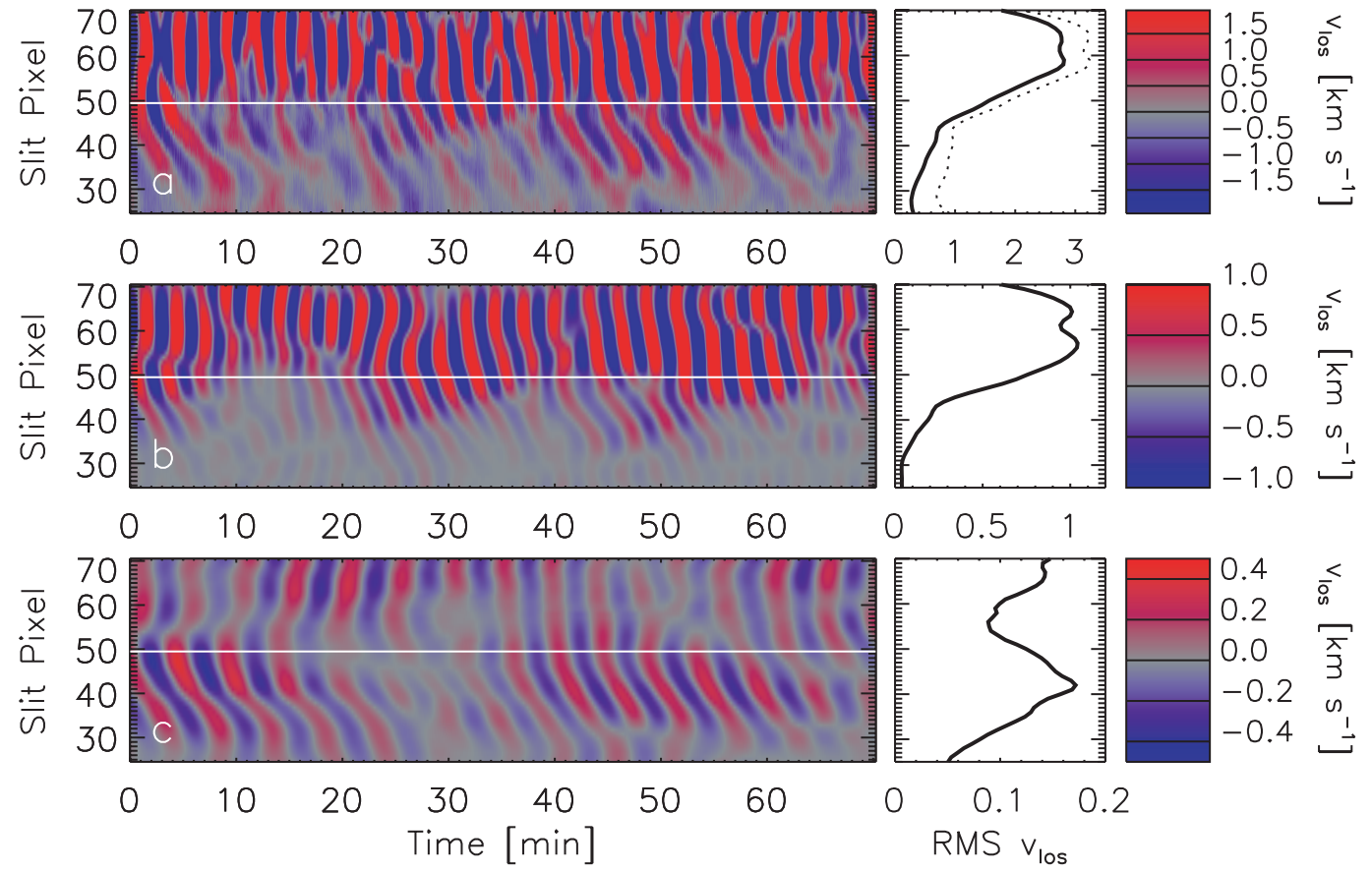

FIG. 6.—Space-time plots covering the sunspot umbra and penumbra. (*a*) He I velocities retrieved by the inversion. (*b*) He I velocities after bandpass filtering in the range 2.5–3.5 minutes. (*c*) He I velocities after bandpass filtering in the range 4.5–5.5 minutes. Values in panels *a* and *b* are clipped to enhance wave front visibility within the penumbra. White lines mark the umbra/penumbra boundary, while right-hand panels show unclipped rms LOS velocity. The dotted curve included in the upper RMS velocity panel shows the rms velocity parallel to the field, after cosine correction for the inclination of the field from the observer's LOS.

in Fig. 6*a* shows that the RMS LOS velocity decreases throughout the penumbra. However, the correct quantity to consider is the rms velocity along the magnetic field vector. This was obtained from the rms LOS velocity (right-hand panel of Fig. 6*a*, *solid curve*) using the measured field inclinations from the observer's LOS–resulting field-aligned RMS velocities are depicted in Figure 6*a* by a dotted curve. The field-aligned rms velocities still show a decrease close to the umbra/penumbra boundary (from a greatly diminished contribution of transmitted power at 3 minute period) but also a nearly constant value of $\sim$1 km s^{-1} over pixels 45 to 25 of the penumbra, lending more credence to the "visual pattern" scenario.

Our results support the conclusion of Kobanov et al. (2006) that 3 minute umbral waves are not the source of 5 minute RP waves. However, we have additionally shown that they are in fact different manifestations of the same form of wave generated by a common source at the photosphere, their differences arising from the transmitted wave power available for propagation along differently inclined field lines. As such, the observed behavior of waves in both umbrae and penumbrae can be explained without the need for abrupt changes in either density or field orientation at the umbra/penumbra boundary as postulated by, e.g., Tziotziou et al. (2006, 2007).

5. CONCLUSIONS

We have provided evidence that velocity signatures of RP waves observed in the He I λ10830 multiplet are more compatible with upward-propagating waves than with trans-sunspot waves through careful consideration of the magnetic vector. Comparing the Fourier phase differences measured between paired pixels in the photosphere and chromosphere to the dispersion relation for field-aligned acoustic waves, modified for inclined fields, points toward such waves (i.e., essentially low-β slow modes) being responsible for the visual pattern.

Initially excited by a common source at the photosphere, waves experience increasing path length to the sampling height in the chromosphere with distance into the penumbra from traveling along increasingly inclined field lines—a scenario previously suggested by, e.g., Rouppe van der Voort et al. (2003) and Bogdan & Judge (2006). For essentially constant (or weakly increasing) propagation velocities, delays of increasing magnitude will be observed in the arrival times of wave fronts at increasing radial distance through sunspot penumbrae. It is the pattern of delayed wave fronts that gives rise to the apparent outward motion of RP waves which may also explain the large range of observed wave speeds—the horizontal "speed" of the delayed wave fronts at the chromosphere depends on the rate at which the magnetic field inclines out through penumbrae, permitting either subsonic or supersonic horizontal "speeds" for different magnetic geometries. This scenario also indicates that RP waves may occur at the edges of large pores since the existence of a penumbra is not necessary to support them; only sufficiently inclined field lines are required to direct the waves laterally.

The German Vacuum Tower Telescope is operated on Tenerife by the Kiepenheuer Insitute in the Spanish Observatorio del Teide of the Instituto de Astrofísica de Canarias. The authors wish to extend their sincere thanks to R. Centeno, M. Collados, and J. Trujillo Bueno for providing this excellent data set for our analysis.

REFERENCES

Ballesteros, E., Collados, M., Bonet, J. A., Lorenzo, F., Viera, T., Reyes, M., & Rodriguez Hidalgo, I. 1996, A&AS, 115, 353
Bel, N., & Leroy, B. 1977, A&A, 55, 239
Bogdan, T. J., & Judge, P. G. 2006, Philos. Trans. R. Soc. London A, 364, 313
Centeno, R., Collados, M., & Trujillo Bueno, J. 2006, ApJ, 640, 1153
Christopoulou, E. B., Georgakilas, A. A., & Koutchmy, S. 2000, A&A, 354, 305
———. 2001, A&A, 375, 617
Collados, M. V. 2003, Proc. SPIE, 4843, 55
De Pontieu, B., Erdélyi, R., & James, S. P. 2004, Nature, 430, 536
Georgakilas, A. A., Christopoulou, E. B., & Koutchmy, S. 2000, A&A, 363, 306
Giovanelli, R. G. 1972, Sol. Phys., 27, 71
Jensen, E., & Orrall, F. Q. 1963, ApJ, 138, 252
Kobanov, N. I., & Makarchik, D. V. 2004, A&A, 424, 671
———. 2006, Sol. Phys., 238, 231
Krijger, J. M., Rutten, R. J., Lites, B. W., Straus, T., Shine, R. A., & Tarbell, T. D. 2001, A&A, 379, 1052
Lagg, A., Woch, J., Krupp, N., & Solanki, S. K. 2004, A&A, 414, 1109
Lagg, A., Woch, J., Solanki, S. K., & Krupp, N. 2007, A&A, 462, 1147
Lites, B. W. 1984, ApJ, 277, 874
Martínez Pillet, V., et al. 1999, in ASP Conf. Ser. 183, High Resolution Solar Physics, ed. T. R. Rimmele, K. S. Balasubramaniam, & R. R. Radick (San Francisco: ASP), 264
Rouppe van der Voort, L. H. M., Rutten, R. J., Sütterlin, P., Sloover, P. J., & Krijger, J. M. 2003, A&A, 403, 277
Rüedi, I., Solanki, S. K., & Livingston, W. C. 1995, A&A, 293, 252
Sivaraman, K. R. 1973, Sol. Phys., 33, 333
Tziotziou, K., Tsiropoula, G., Mein, N., & Mein, P. 2006, A&A, 456, 689
———. 2007, A&A, 463, 1153
Wikstøl, Ø., Hansteen, V. H., Carlsson, M., & Judge, P. G. 2000, ApJ, 531, 1150
Zirin, H., & Stein, A. 1972, ApJ, 178, L85